Forward Flight Rotor Performance at Martian Atmospheric Densities and Sensitivity to Low Reynolds Numbers

Brenda Natalia Perez Perez
brenda.n.perezperez@nasa.gov
Aerospace and Mechanical Engineer
Science and Technology Corporation
NASA Ames Research Center, Moffett Field, California

ABSTRACT

Much effort has been made to enhance exploration on Mars. In addition to a rover and Mars-orbiting satellites, a Mars Helicopter Technology Demonstrator was proposed by the NASA Jet Propulsion Laboratory (JPL) to augment planetary research for the Mars 2020 Mission. Understanding rotor performance is vital for operations at Martian atmospheric conditions. The work presented is a study investigating rotor performance at Martian atmospheric conditions. Forward flight rotor tests were conducted in the Planetary Aeolian Laboratory (PAL) at NASA Ames Research Center, which has the capability to evacuate the air in the chamber to reach Martian atmospheric densities. A 1-meter-diameter rotor, roughly approximating the Mars Helicopter Technology Demonstrator, was tested at multiple atmospheric densities, including that of Mars. Rotor rotational speed, thrust, torque, power, and airspeed measurements were collected during the test. These results were then correlated with simulated cases using a mid-fidelity computational fluid dynamics software, Rotorcraft CFD (RotCFD). C81Generator (C81Gen) was used to generate airfoil aerodynamic coefficient for the spanwise locations along the rotor. To observe the differences between the C81Gen flow type modes at low Reynolds number, the simulations at Martian atmospheric densities were run under the "fully turbulent", and the fully laminar flow type. In addition, Reynolds number effects (within $2x10^4$ to $9x10^4$) on experimental thrust coefficient, power coefficient, and figure of merit were analyzed. Within this chord- based Reynolds number range, C_T and FM decreased around 26% and 36%, respectively, while C_P remained fairly constant, exhibiting variations of no more than 5.5%. Despite the challenges involved in testing at a large difference of atmospheric densities between Earth and Mars, repeatable data was obtained in all the measurements at Martian atmospheric conditions.

NOTATION

C_P	Rotor power coefficient
C_T	Rotor thrust coefficient
FM	Figure of merit
$Re_{0.75R}$	Reynolds number at 75% radial station
V_h	Induced velocity
V_m	Measured experimental wind speed
V_{tip}	Tip speed
μ	Advance ratio

ARC2D	Two-Dimensional Navier–Stokes Flow Solver
BEM	Blade-Element Model
C81Gen	C81 Generator
CAD	Computer-Aided Design
CFD	Computational Fluid Dynamics
DAS	Data Acquisition System
JPL	Jet Propulsion Laboratory
MARSWIT	Martian Surface Wind Tunnel
MC	Martian Conditions
MH	Mars Helicopter
PAL	Planetary Aeolian Laboratory
RANS	Reynolds-Averaged Navier–Stokes
RNE	Reynolds Number Effect
RotCFD	Rotorcraft CFD
RotUNS	Rotorcraft Unstructured Solver
SA	Spalart–Allmaras
SIMPLER	Semi-Implicit Method for Pressure-Linked Equations Revised
SVS	Steam Vacuum System
TBR	Two-Bladed Rotor
TC	Terrestrial Conditions
URANS	Unsteady Reynolds-Averaged Navier–Stokes

INTRODUCTION

The Mars Helicopter (MH) is a small autonomous vehicle designed to fly near the Martian surface and was a collaborative effort between the JPL, NASA Ames, Langley, and Glenn Research Centers, and AeroVironment Inc. The vehicle will be included in the 2020 mission to Mars and serve as a technology demonstrator to augment planetary research. The MH will enhance current exploration

Presented at the VFS Aeromechanics for Advanced Vertical Flight Technical Meeting, San Jose, CA, January 21–23, 2020.

capabilities of Mars-orbiting satellites and rovers by providing larger visual range while allowing for imagery resolutions comparable to those seen in the rovers and landers [1]. Within its operation, the MH is designed to fly at airspeeds that do not exceed 10 m/s horizontally [2]. This technology has sparked interest for future Martian rotorcraft development. However, testing and measuring rotor forward flight performance at Martian atmospheric conditions is a relatively unexplored area. Therefore, an experimental study was performed in a wind tunnel to investigate rotor forward flight performance, and demonstrate successful rotor operation at Martian atmospheric densities and at airspeeds below 10 m/s. Experiments were conducted in a facility capable of evacuating the air to achieve the thin Martian atmosphere of approximately 1% of Earth's atmospheric density. Simulations and testing of rotors are vital for evaluating rotor performance and behavior; thus, experimental results were then compared with simulated cases using a mid-fidelity computational fluid dynamics tool, Rotorcraft CFD. In addition, Reynolds number effects on experimental thrust and power coefficients were analyzed for both two- and four-bladed rotor configurations at pressures ranging from 40 to 193 mbar.

MARTIAN ATMOSPHERIC CONDITIONS

The thin Mars atmosphere of approximately 1% of Earth's sea level atmospheric density makes flying a challenging task. The Martian atmosphere is composed of 95% CO_2, with the remaining 5% comprised of N_2 and other trace gases. Mars' gravity is slightly greater than one-third of Earth's, and the surface temperature is about -60 degrees Celsius. A seasonal variation of approximately 20% of the planetary atmospheric mass occurs on Mars because of polar CO_2 condensation and sublimation [3].

ATMOSPHERIC DENSITY CONDITIONS IN EXPERIMENT

Atmospheric conditions expected on Mars during the daytime include densities ranging from 0.014 to 0.02 kg/m^3 [1], which are the densities in which the MH is designed to operate [2]. The rotors in this experiment were tested within a similar range of Martian Conditions (MC) in addition to Terrestrial Conditions (TC) (see Table 1). Condition 1 and 2 refers to the two- and four- bladed rotors respectively. In addition, both rotor configurations were tested over a pressure range to analyze Reynolds Number Effect (RNE) on rotor performance.

Work by Anyoji et al. [4] on tested airfoils in both CO_2 and air at low Reynolds number did not exhibit significant heat ratio effects on aerodynamic performance. Further, previous work shows that temperature effects cause a minor effect on rotor performance in simulations. Koning and Johnson [5] analyzed the influence of low temperatures on their CFD rotor models for the MH by comparing two models at 20 °C and -50 °C at Martian atmospheric conditions. Results showed that both models perform similarly over the design thrust coefficient range, and when comparing the lower temperature model with experimental measurements at 20 °C, the figure of merit is shown to be 1.3 to 2.6% higher over the design thrust coefficient range of the MH. The large change in density between the Martian and terrestrial atmosphere is thought to be the main parameter affecting rotor aerodynamic performance. No attempt was made to model Martian composition or temperature in this project; at all atmospheric conditions, the PAL chamber composition was that of Earth's.

Table 1. Atmospheric density and pressure conditions in the experiment.

Variable	TC1	TC2	MC1	MC2	RNE
Density (kg/m^3)	1.219	1.230	0.013	0.015	0.053 to 0.228
Pressure (mbar)	1026.8	1022.4	10.7	12.5	43 to 193

EXPERIMENTAL SETUP

The work presented here is an extension of the initial study performed by Ament and Koning [6], where a description of the experimental setup can be found. Information is repeated in this work for the benefit of the reader. However, sections have been modified to describe the distinctive setting conditions of this work.

Planetary Aeolian Laboratory

The PAL is a near-vacuum facility capable of conducting experiments under atmospheric conditions ranging from Earth's atmosphere, approximately 1-bar, down to 5.5 mbar, which is less than the atmospheric pressure of Mars. The PAL has a chamber with an inside height of 30 meters and an inside volume of 4000 cubic meters. The facility can be evacuated to its minimum pressure of 5.5 mbar in about 45 minutes, an operation performed by the NASA Ames Thermal Physics Facility's Steam Vacuum System (SVS) [7]. A picture of the PAL is shown in Figure 1.

Because of the high cost of evacuating the PAL, the majority of the PAL testing is done in conjunction with other NASA Ames projects already requiring vacuum; in doing so, the windows of time allotted to PAL vacuum testing are often based on dual-use opportunities. Although not pursued for

this project, vacuum testing can be dedicated to the PAL if sufficient funding is in place, allowing for extensive low pressure testing.

Figure 1. Planetary Aeolian Laboratory.

Martian Surface Wind Tunnel

The Martian Surface Wind Tunnel (MARSWIT), shown in Figure 2, was first put into operation in 1976, and is an open-circuit 13-m-long atmospheric boundary-layer wind tunnel. The internal cross section is 1 (height) by 1.2 (width) m. As the MARSWIT is located in the PAL near-vacuum chamber, the wind tunnel can be utilized at the same atmospheric conditions as the PAL facility. At one atmosphere, the wind tunnel can reach wind speeds of 10.5 m/s, and at 5.5 mbar it can reach wind speeds of 100 m/s. The tunnel has been used to investigate the physics of particle entrainment under Martian conditions, to test spacecraft instruments under Martian conditions [8], and recently to test rotor performance. All test data presented in this paper was acquired with the wind tunnel drive system turned off.

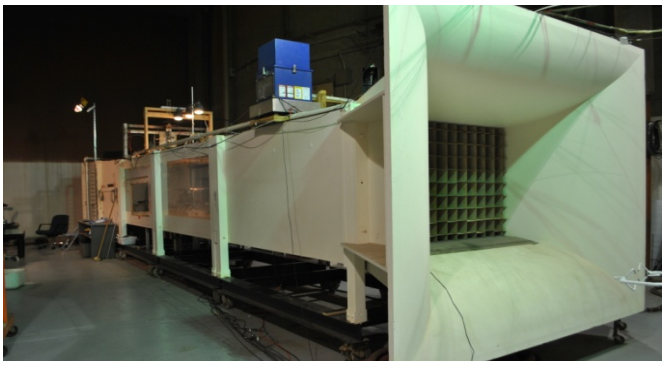

Figure 2. Martian Surface Wind Tunnel inside the PAL.

Test Overview

Test hardware was installed into the MARSWIT test section approximately midway along the 13-m-long wind tunnel. Testing consisted of both two- and four-bladed rotor configurations. The objective of the two-bladed rotor configuration was to test a rotor in nominal helicopter mode. The objective of the four-bladed rotor configuration was to resemble the MH coaxial design, as well as to provide increased rotor thrust representative of the MH design. However, unlike the MH coaxial system, both rotors in the four-bladed configuration are fixed and rotating in the same direction at an orientation of 90 degrees. Both the two- and four-bladed rotor configurations are shown in Figure 3. Test hardware was designed such that the rotor could be tested between ±14 degrees angle of attack.

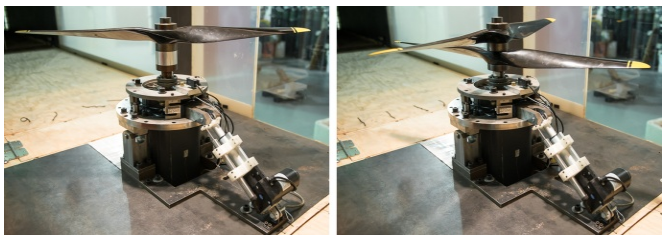

Figure 3. Two-bladed (left) and four-bladed (right) rotor configurations tested in the MARSWIT test section.

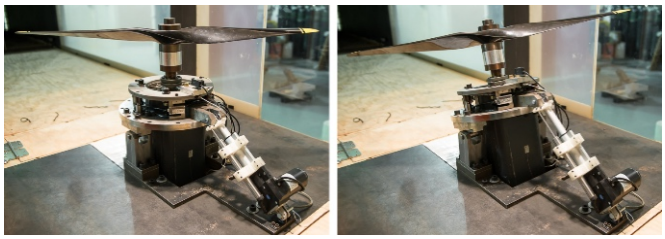

Figure 4. Two-bladed rotor at shaft angle of 0 degrees (left) and two-bladed rotor at shaft angle of -14 degrees (right).

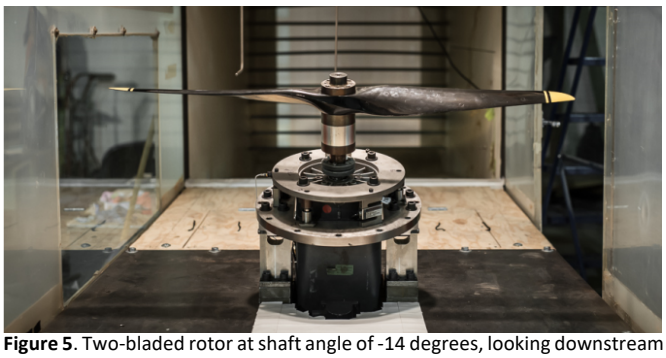

Figure 5. Two-bladed rotor at shaft angle of -14 degrees, looking downstream of the test section.

For the presented data, all tests were conducted at -14 degrees, pitching the test apparatus towards the tunnel inlet. Figure 4 shows the two-bladed rotor configuration at 0 degrees and -14 degrees (forward flight). Figure 5 shows the rotor again at -14 degrees, but from downstream of the test section. Testing was conducted from a pressure range of 1 atmosphere (Earth's atmosphere) down to 10.7 mbar

(conditions that approximate the atmospheric conditions found on Mars).

Test Model Hardware and Sensors

The primary goals of the experiment were to collect rotor thrust, RPM, power, torque, motor temperature, and wind speed, as well as chamber pressure, humidity, and temperature, while in forward flight. The following sections discuss the hardware and sensors used to obtain this data, and Figures 6 and 7 show their location within the MARSWIT.

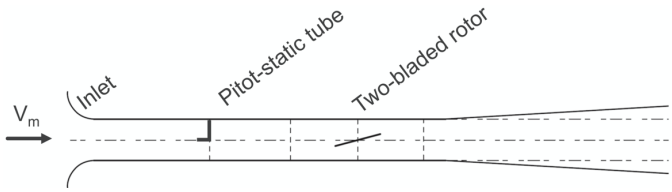

Figure 6. Side profile of the 13-ft-long MARSWIT.

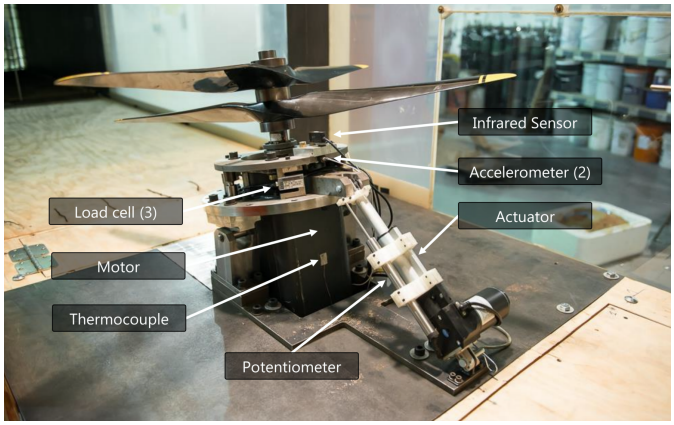

Figure 7. Hardware and sensor installation within the MARSWIT test section.

Prior to MH testing in the JPL 25-Foot Space Simulator, a 1-atmosphere rotor hover safety checkout needed to be conducted within the chamber. As part of this effort, the 40x22 rotor was selected in 2015 and tested for this activity [9]. The same rotor blades and motor were used for reduced pressure forward flight testing at NASA Ames Research Center in 2017.

To provide a better understanding of what the MH might experience during forward flight on Mars, the selected rotor was chosen based on the physical dimensions and operating conditions of the MH. The projected MH will be equipped with a coaxial rotor system, with rotor disks approximately 1.2 m in diameter. However, because of restrictions in MARSWIT test section dimensions, the largest testable rotor was limited to 1 m in diameter, approximately 0.2 m smaller than what will be installed on the MH. In addition to rotor diameter, the selected rotor was chosen to be operational up to 3400 RPM to include the RPM and hover tip Mach number of the proposed MH.

The selected rotor is highly twisted and defined by the manufacturer as 40x22. The first number represents the rotor diameter in inches. The second number refers to the forward distance traversed, in inches, for every rotor revolution when acting as a propeller [10].

The motor used for rotor operation is the Siemens Electric AC Motor, model #1FT5104-0AF71-1. This motor was selected for the first ever Martian atmosphere rotor hover testing in 2002, which also took place in the PAL near-vacuum chamber [11]. Because this motor was proven capable of operating extensively under vacuum, it was chosen again for this test. Measurements in the experiment included RPM based on a motor encoder and torque based on motor current; both RPM and torque were recorded by the Data Acquisition System (DAS). A thermocouple was mounted to the motor for temperature monitoring.

An Omron #E3S-AR11 infrared sensor (IR) was used during testing. This is a built-in amplifier photoelectric feedback sensor, which was used to indicate motor RPM. Reflective tape, adhered to the motor shaft, reflects the IR signal once per motor revolution. This sensor was only used to monitor RPM while testing and was not recorded.

To measure rotor thrust, the motor is fixed to three Sensortronics S-Beam load cells, model #60001. Each load cell is single axis and can measure up to 220 N within a safe margin. The collective 660 N measurable weight is required to accommodate the dead weight of the motor and rotor hardware. The load cells were mounted 120 degrees apart about the rotor's axis of rotation.

MARSWIT wind speed is determined from two differential pressure transducers; a ± 1.25 mbar (Setra 239) and 1 mbar (Barocel-590) range. These were attached to pitot-static probes located forward of the test section. The Barocel-590 was only used for 1 atmosphere measurements. Wind speed is measured only in the direction of air entering the MARSWIT inlet.

To determine the test hardware structural resonance, a resonant frequency test was performed for each rotor configuration. Frequencies with the highest amplitude occur around 1900 RPM for the two- and four-bladed rotor configurations.

Vibrations were monitored throughout testing by two uniaxial 5-g Kistler accelerometers mounted 90 degrees apart, on a plane perpendicular to the axis of rotation. Accelerometer installation was for the sole purpose of monitoring amplitude throughout testing, particularly around determined resonant frequencies.

Absolute chamber pressure, density, humidity, and temperature sensors located in the PAL vacuum chamber

were used for this test. The Setra 204 absolute pressure transducer and a Wallace and Tiernan FA129 absolute pressure gauge were used to measure chamber pressure for pressures ranging from 1 atmosphere to around 5.5 mbar. One MKS Baratron 627F 0-13 mbar absolute pressure transducer is used when low pressures are reached. Lastly, humidity and temperature were measured by a Vaisala DMP248.

Data Acquisition Systems

All sensor cables bridge the vacuum chamber wall to the PAL control room, where they are recorded to one of two data systems, an AstroMed Dash 18X (AstroMed) and a PAL LabVIEW system. The AstroMed is a 14-bit DAS used for real-time monitoring and data recording, with real-time sensor calibration and filter application. Rotor thrust, RPM, power, torque, wind speed, and stand vibration were recorded to this system. The PAL LabVIEW system recorded absolute chamber pressure, density, humidity, and temperature.

Post-processed data records are merged based on the time stamp of each DAS. Once merged, the data undergoes zero-point subtraction of load cell weight, and torque tares.

Chamber Testing Conditions

Figures 8 and 9 show PAL chamber pressure against the time between data points collected for two- and four-bladed rotor configurations over the course of a single chamber pressure cycle. Collected data can be broken into four facility operational categories: pressure decrease, constant pressure (holding pressure), pressure drift, and pressure increase.

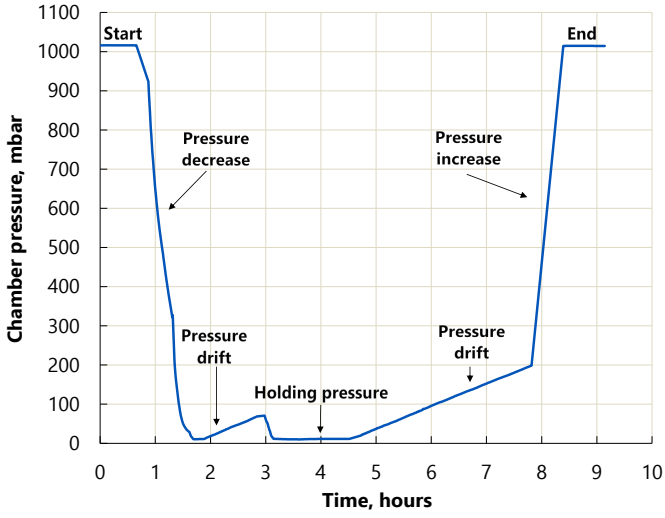

Figure 8. PAL absolute chamber pressure plotted against the time two-bladed rotor data was collected.

Pressure Decrease

Pressure decrease is the condition when the PAL evacuates the air from 1 atmosphere to reach Martian atmospheric densities.

Constant Pressure

When reduced pressures are reached, and the PAL is closed off from the SVS, the facility leaks at about 1 mbar per minute. Thus, to hold constant pressures, the facility operator manually regulates the opening of the valve until the desired pressure is steady. However, once manual regulation of the valve ceases, the pressure can deviate up to 5% from the steady pressure reached in some instances. Currently, there is no automatic device controlling the valve that can rapidly account for the loss of pressure and set the valve to a desired position.

For the two- and four-bladed rotor, the pressure was held constant at roughly 10.7 and 12.5 mbar, respectively.

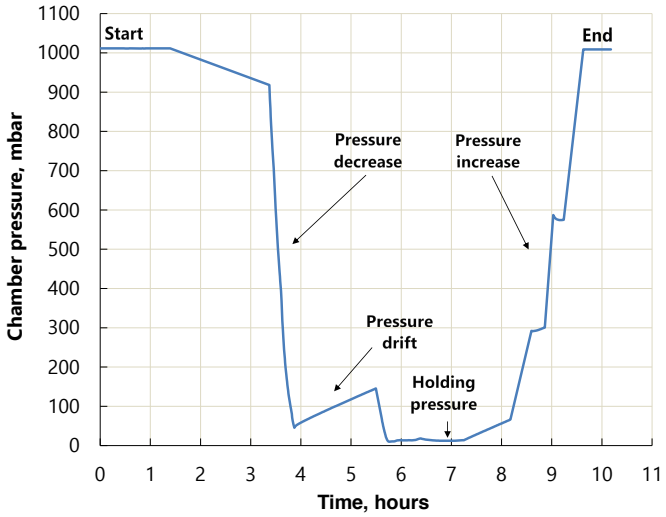

Figure 9. PAL absolute chamber pressure plotted against the time four-bladed rotor data was collected.

Pressure Drift

When the PAL vacuum is shut off, pressure within the PAL can be sustained, but experiences a drift at a rate of approximately 1 mbar per minute. To provide an ample amount of data points while simultaneously minimizing the amount of pressure drift, 15-second data points were collected; this corresponded to approximately 0.25-mbar drift for each data point collected. While PAL pressure drifted, data was collected successively for both two- and four-bladed rotors over a pressure range of 43 to 193 mbar.

Pressure Increase

When the PAL vacuum is shut off, and reduced pressure tests are concluded, the valve of the facility is opened to reach 1 atmosphere.

SIMULATIONS

The experimental results were compared against RotCFD simulations at 1 atmosphere, 12.5 mbar, and 10.7 mbar.

RotCFD is a mid-fidelity CFD tool specifically designed for rotorcraft design efforts [12]. The Rotorcraft Unstructured Solver (RotUNS) is a module within RotCFD that solves the three-dimensional (3D) incompressible Unsteady Reynolds-Averaged Navier–Stokes (URANS) equations on a Cartesian unstructured grid using an implicit finite-volume method. The Semi-Implicit Method for Pressure-Linked Equations Revised (SIMPLER) is used to link the equations. Turbulence is modeled in RotCFD using the k-ε turbulence model with special wall function. A rotor is modeled using a Blade-Element Model (BEM) and interacts with the flow-field through the momentum it imparts on the flow. RotCFD has been successfully used for various analyses on complex rotor flows [13][14] at a fraction of the computational budget when compared to a complete Navier–Stokes solution for a rotating body-fitted rotor.

CFD Approach

RotCFD requires a set of aerodynamic coefficients for the airfoil sections corresponding to the experiment conditions. Therefore, the rotor blade was 3D scanned to obtain the aerodynamic coefficients in C81 Generator (C81Gen) from the airfoil sections. This process is described in the following section.

3D scanning

To generate the CFD airfoil tables for the rotor, the blade was measured using the CreaformMetraScan-70, a 3D optical laser scanner. The resulting point cloud was processed by fitting profile curves and surfaces to reconstruct the 3D CAD model of the rotor [10] (see Figure 10). The airfoils were used to extract the magnitude and location of maximum thickness and camber to evaluate the critical radial station selection. Radial stations at r/R = 0.21, 0.29, 0.74, and 0.95 were chosen as the critical airfoils.

Aerodynamic coefficients

C81Generator (C81Gen) is used to generate aerodynamic coefficients for spanwise locations along the rotor. C81Gen is developed to create C81 format tables for a user-specified range of angle-of-attack/Mach pairs. C81Gen runs the two-dimensional, time-dependent compressible Reynolds-Averaged Navier–Stokes (RANS) solver ARC2D with structured body-fitted viscous gridding. The program uses an implicit finite-difference method to solve two-dimensional thin-layer Navier–Stokes equations [15]. In C81Gen the flow type can be set to "fully turbulent" using Spalart–Allmaras (SA) turbulence model, fully laminar, or set to use prespecified transition locations.

The critical Reynolds number occurs around 10^5 for slender streamline shapes [16]. The operational chord-based Reynolds number of the airfoils in the experiment at Martian atmospheric densities ranges from around 1500 to 7000. To observe the differences between the fully laminar and "fully turbulent" flow types at low Reynolds number in C81Gen, the simulations at Martian atmospheric densities were run under both conditions. In the one atmosphere cases, the flow type of the airfoils was set to "fully turbulent".

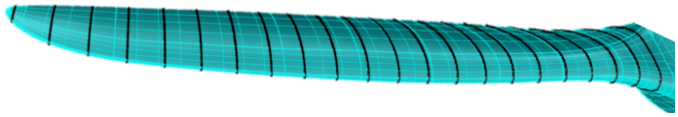

Figure 10. Rotor CAD model for airfoil extraction.

Grid settings in this study are the same as those determined by Koning in his grid resolution study for the airfoil sections of this rotor [10]. C-grids were used, and all airfoils had normalized chord lengths of c = 1.0 with the far field located at 50c. For the C-grid, the number of points in the streamwise, normal, and wake direction were 501, 167 and 83, respectively. The y^+ value was kept around y^+ = 1.0 for all cases investigated (see Figure 11). Airfoil tables at terrestrial and Martian atmospheric densities (1.225 and 0.016 kg/m^3, respectively) were generated and used in this study.

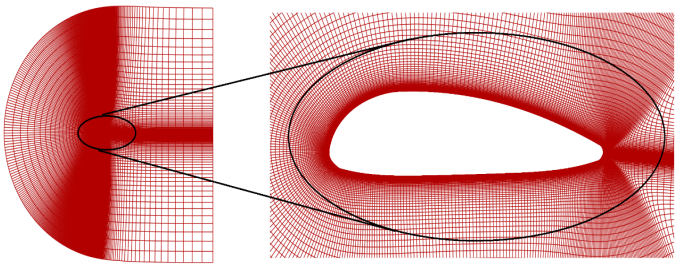

Figure 11. Close view of C81Gen grid.

RotCFD simulation

In the RotCFD simulation, the uniform boundaries have the same cross section dimensions as the MARSWIT, and they were set to viscous walls to simulate the wind tunnel. Analogous to the rotor in the experimental setup, the rotor in

the simulation was placed inside the wind tunnel at -14 degrees pitch. The inlet boundary condition was set to the velocities measured from the experimental testing. A detailed description of additional simulation settings, as well as the simulation approach, can be found in the work by Perez Perez [17]. This included an analysis to find the most optimal simulation settings for these experiments at both 1 atmosphere and reduced pressure conditions in RotCFD. In Perez Perez [17], an idealized geometry of the motor was used in the simulations to analyze the effects of the motor blockage. However, in this work the motor and the motor disk assembly were modeled as seen in the experiment. Figure 12 shows the grid in the MARSWIT test section near the rotor, and Figure 13 shows a representation of the flow visualization of the two-bladed rotor at 10.7 mbar and 2000 RPM velocity field.

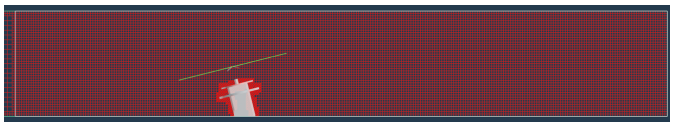

Figure 12. Section of RotCFD grid near the two-bladed rotor in MARSWIT test section. Tunnel wind direction is left to right.

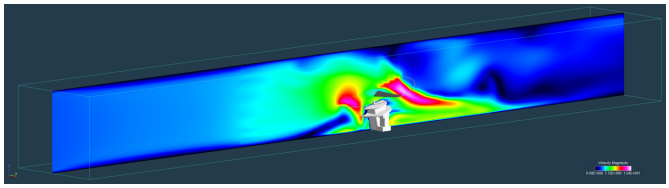

Figure 13. Flow visualization of velocity field (label is in meters per seconds). Two-bladed rotor operating at 10.7 mbar and 2000 RPM.

RESULTS

This section shows rotor performance in terms of thrust, torque, and power for two- and four-bladed rotors at terrestrial and Martian atmospheric densities. These performance results were compared against CFD simulations. In addition, Reynolds number effect on experimental thrust, power coefficient, and figure of merit is shown for the two- and four-bladed rotor at pressures ranging from 40 to 193 mbar. Lastly, C81Gen drag and lift coefficient results at Martian atmospheric densities are shown for r/R=0.74 at Mach 0.2 and 0.5 to show the difference between the "fully turbulent" and fully laminar flow type.

The forward flight experimental data of the testing performed from one atmosphere to Martian atmospheric densities for the two- and four-bladed rotor can be found in Perez Perez, Ament and Koning [18]. The forward flight two-bladed rotor data at one atmosphere shown in the following sections was acquired from Ament, Koning and Perez Perez [19].

EXPERIMENTAL RESULTS

Two-bladed rotor at terrestrial atmospheric densities

The two-bladed rotor was operated from 500 to 2200 RPM. Figure 14 shows the wind speeds reached at each tip speed. The rotor results exhibited representative behavior of a helicopter in hover. Table 2 shows a wind speed analysis to demonstrate such behavior. In Table 2, calculated induced velocities (V_h, from a rotor in hover) increase as the tip speed increases (V_{tip}). However, the ratio of the measured experimental wind speed (V_m) over induced velocity was kept roughly constant. Similarly, the advance ratio (μ) stays fairly constant and close to zero, which is comparable to the behavior of a rotor in hover. This behavior was consistent for measurements at terrestrial and Martian atmospheric densities. A similar analysis is provided in Tables 3, 4, and 5 for each case shown in this work. Thrust and torque are expected to be linear with RPM^2 for a purely hovering rotor, which was shown to be true for measurements at terrestrial and Martian atmospheric densities in forward flight. This is shown in plots of thrust and torque vs. RPM^2 on Figures 15, 16, 19, and 20 for terrestrial conditions, and 23, 24, 26, and 27 for Martian conditions. The low and almost constant advance ratio for all test conditions allowed for the linear thrust variation with RPM^2 at these low pressures.

The two- and four-bladed rotors were also tested in a hover configuration, as seen in Argus, Ament and Koning [20]. The thrust, torque and power results from that hover experiment are shown in Figures 15 to 17 and 19 to 21 to compare with the forward flight results presented herein. The similarity between the thrust, torque and power data further confirms that the rotors in forward flight of this experiment exhibited a behavior representative of the rotors in hover.

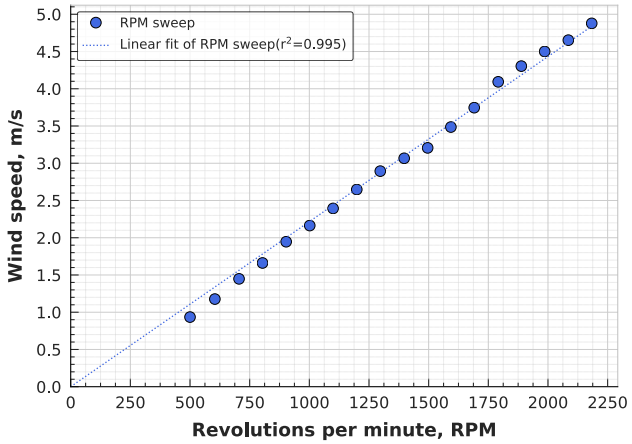

Figure 14. Plot of two-bladed rotor wind tunnel speeds at 1 atmosphere at each tip speed.

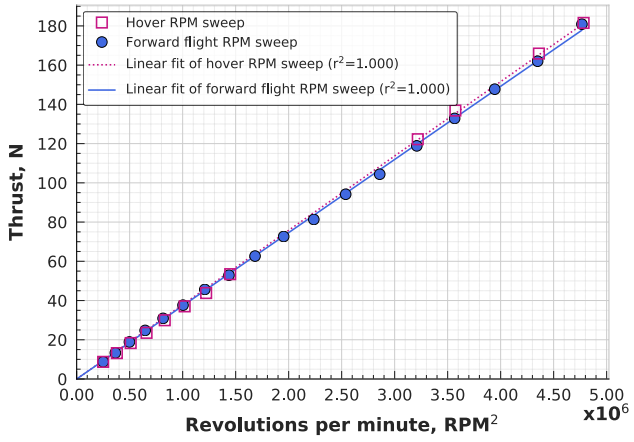

Figure 15. Plot of thrust vs. RPM² for the two-bladed rotor at 1 atmosphere.

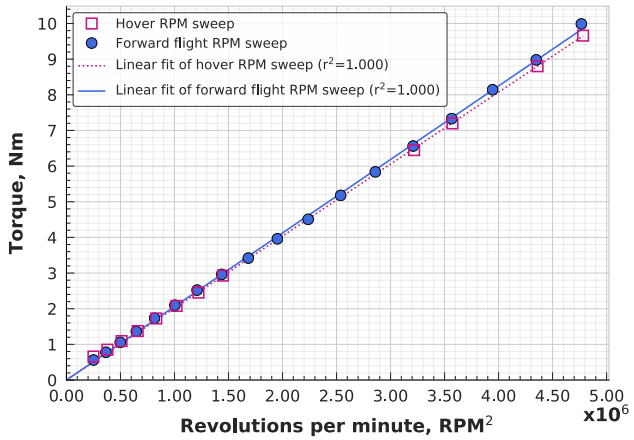

Figure 16. Plot of torque vs. RPM² for the two-bladed rotor at 1 atmosphere.

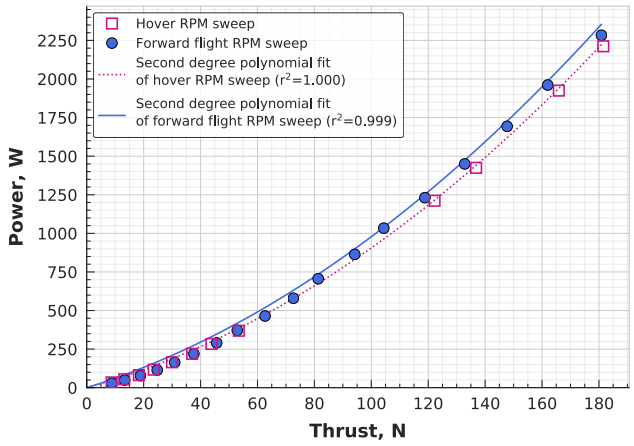

Figure 17. Plot of power vs. thrust for two-bladed rotor at 1 atmosphere.

Table 2. Two-bladed rotor test conditions at 1 atmosphere.

RPM	V_{tip} (m/s)	V_m (m/s)	Calculated V_h (m/s)	$\frac{V_m}{V_h}$	μ
500	26.7	0.9	2.1	0.45	0.035
600	32.1	1.2	2.6	0.46	0.037
700	37.4	1.4	3.1	0.47	0.039
800	42.8	1.7	3.5	0.47	0.039
900	48.1	1.9	3.9	0.50	0.040
1000	53.5	2.2	4.3	0.50	0.040
1100	58.8	2.4	4.8	0.50	0.041
1200	64.2	2.6	5.1	0.52	0.041
1300	69.5	2.9	5.6	0.52	0.042
1400	74.8	3.1	6.0	0.51	0.041
1500	80.2	3.2	6.4	0.50	0.040
1600	85.5	3.5	6.9	0.51	0.041
1700	90.9	3.7	7.2	0.52	0.041
1800	96.2	4.1	7.7	0.53	0.043
1900	101.6	4.3	8.1	0.53	0.042
2000	106.9	4.5	8.6	0.52	0.042
2100	112.3	4.7	9.0	0.52	0.041
2200	117.6	4.9	9.5	0.51	0.041

Four-bladed rotor at terrestrial atmospheric densities

The four-bladed rotor was operated from 600 to 2000 RPM. Figure 18 shows the wind speeds reached at each tip speed. Two- and four-bladed rotors exhibited roughly the same ratio of V_m over V_h (see Tables 2 and 3). The following plots (Figures 19 to 21) show rotor performance results of the four-bladed rotor at 1 atmosphere.

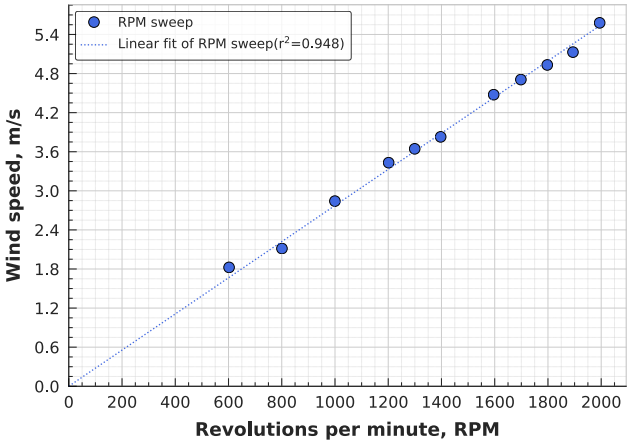

Figure 18. Plot of four-bladed rotor wind tunnel speeds at 1 atmosphere at each tip speed.

Table 3. Four-bladed rotor test conditions at 1 atmosphere.

RPM	V_{tip} (m/s)	V_m (m/s)	Calculated V_h (m/s)	$\frac{V_m}{V_h}$	μ
600	32.1	1.8	3.3	0.56	0.057
800	42.8	2.1	4.5	0.47	0.049
1000	53.4	2.8	5.6	0.51	0.053
1200	64.2	3.4	6.8	0.51	0.053
1300	69.5	3.6	7.3	0.50	0.052
1400	74.8	3.8	8.0	0.48	0.051
1600	85.5	4.5	9.1	0.49	0.052
1700	90.9	4.7	9.7	0.49	0.052
1800	96.2	4.9	10.3	0.48	0.051
1900	101.6	5.1	10.8	0.48	0.050
2000	106.9	5.6	11.4	0.49	0.052

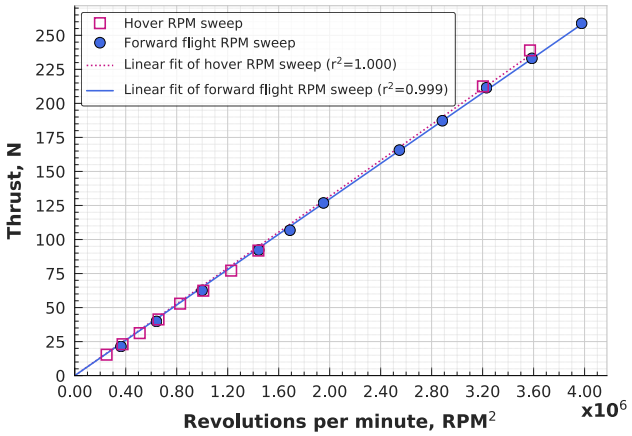

Figure 19. Plot of thrust vs. RPM^2 for the four-bladed rotor at 1 atmosphere.

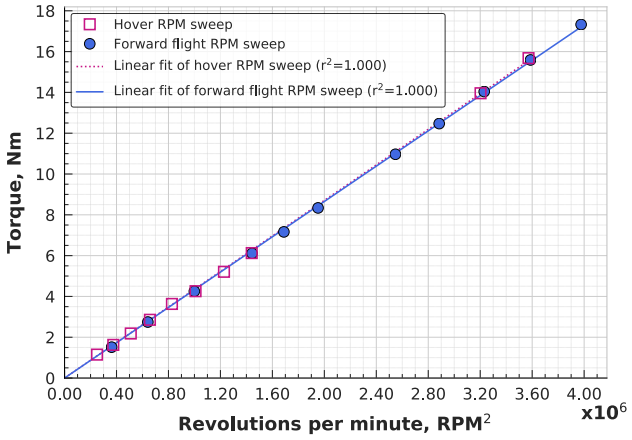

Figure 20. Plot of torque vs. RPM^2 for the four-bladed rotor at 1 atmosphere.

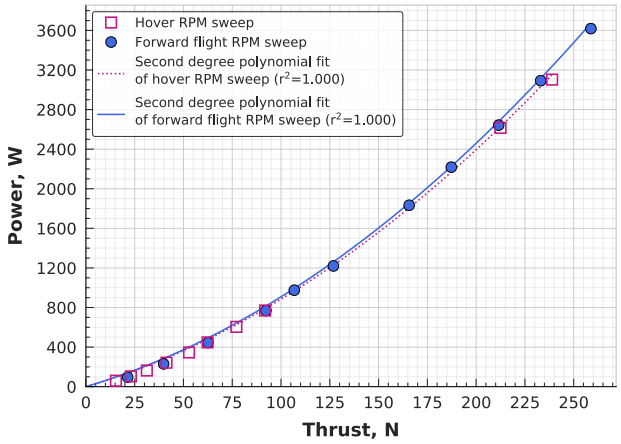

Figure 21. Plot of power vs. thrust for the four-bladed rotor at 1 atmosphere.

Two-bladed rotor at Martian atmospheric densities

The two-bladed rotor was operated from 2000 to 3400 RPM and chamber pressure was held constant at roughly 10.7 mbar. To demonstrate repeatability, two separate RPM sweep sets are shown in this work. Repeatability was demonstrated for thrust, torque, power, and wind speed measurements, where difference between the results exhibited an average of no more than 5%. At such reduced pressures, a difference of 5% at the highest RPM of each measurement represent values of 0.15 N, 0.02 Nm, 6.3 W, and 0.28 m/s.

Figure 22 shows the wind speeds reached at each tip speed. Rotor performance plots at 10.7 mbar for the two-bladed rotor are shown in Figures 23 to 25.

Four-bladed rotor at Martian atmospheric densities

The four-bladed rotor was operated from 2800 to 3400 RPM and chamber pressure was held constant at roughly 12.5 mbar. Rotor performance was measured for this test but wind speed data was not collected. Nonetheless, at 1 atmosphere, two- and four-bladed rotors exhibited a fairly constant ratio of V_m over induced velocity for a corresponding RPM. Moreover, this ratio is kept roughly constant at 1 atmosphere and 10.7 mbar. Therefore, it is expected that the four-bladed rotor exhibited a similar behavior. Hence, in Table 5 the ratio of wind speed over induced velocity at 10.7 mbar for the Two-Bladed Rotor (TBR) was used for this case to predict the wind speed for the four-bladed rotor. Rotor performance plots at 12.5 mbar for the four-bladed rotor are shown in Figures 26 to 28.

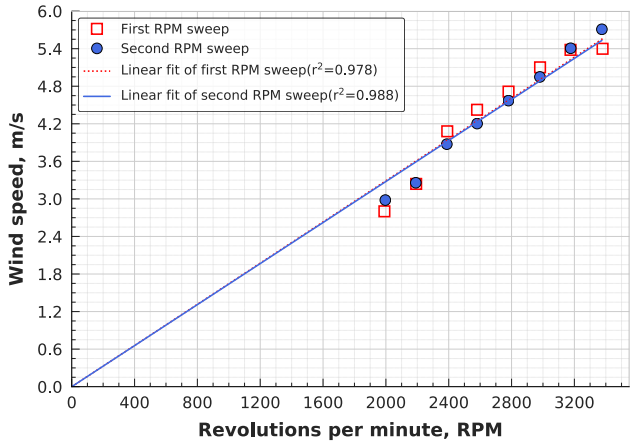

Figure 22. Plot of two-bladed rotor wind tunnel speeds at 10.7 mbar at each tip speed.

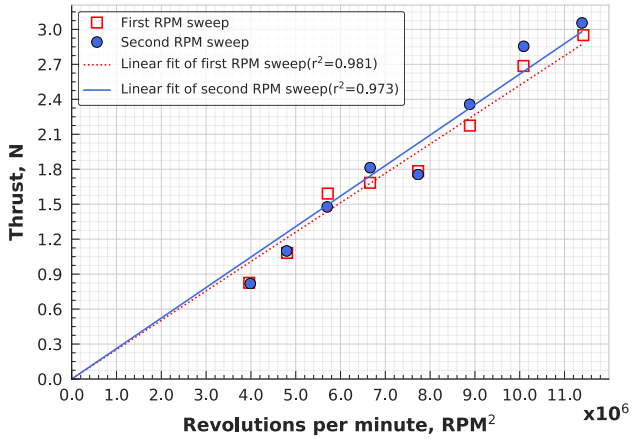

Figure 23. Plot of thrust vs. RPM² for the two-bladed rotor at 10.7 mbar.

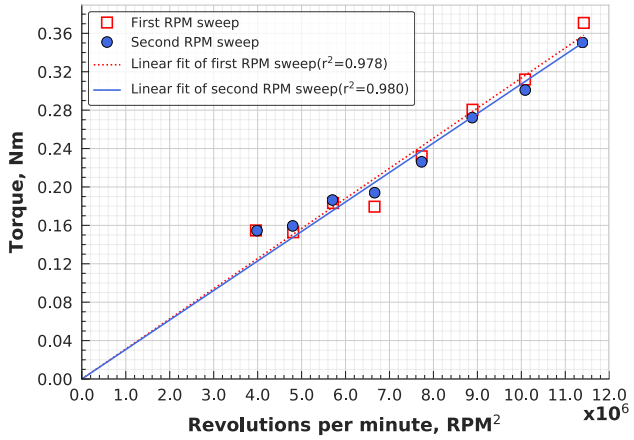

Figure 24. Plot of torque vs. RPM² for the two-bladed rotor at 10.7 mbar.

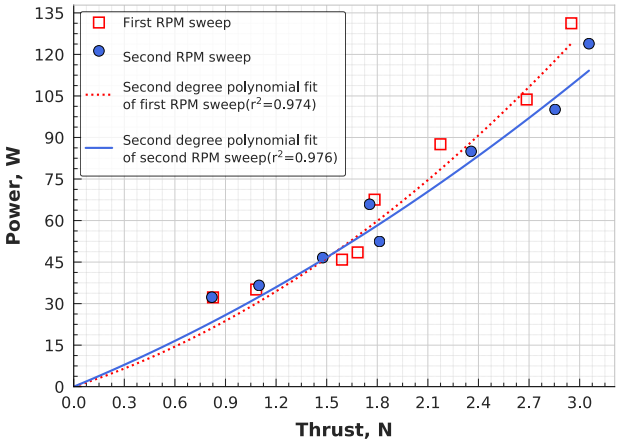

Figure 25. Plot of power vs. thrust for the two-bladed rotor at 10.7 mbar.

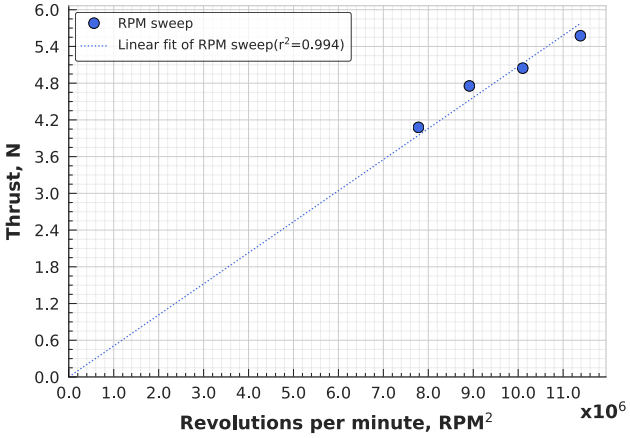

Figure 26. Plot of thrust vs. RPM² for the four-bladed rotor at 12.5 mbar.

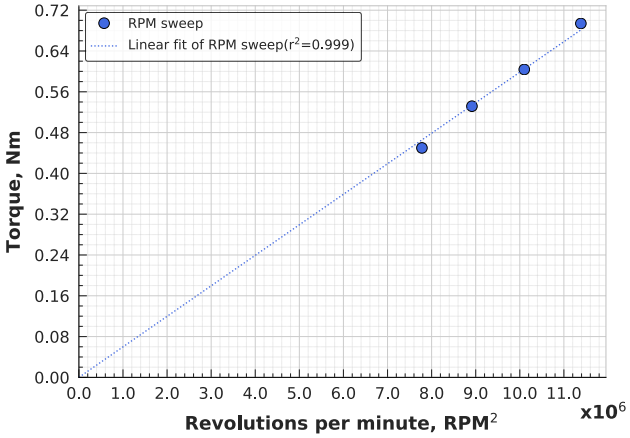

Figure 27. Plot of torque vs. RPM² for the four-bladed rotor at 12.5 mbar.

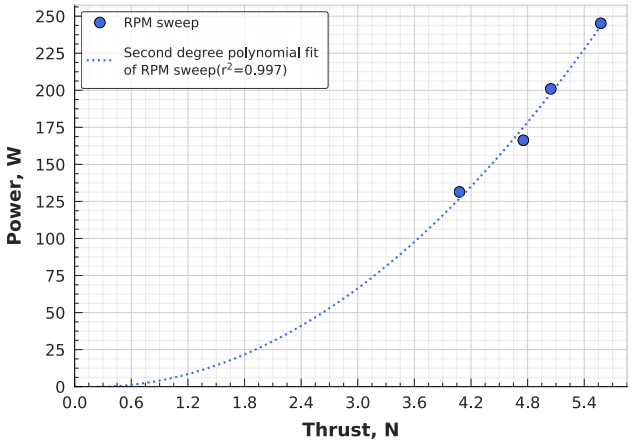

Figure 28. Plot of power vs. thrust for the four-bladed rotor at 12.5 mbar.

Table 4. Two-bladed rotor test conditions at 10.7 mbar.

RPM	V_{tip} (m/s)	V_m (m/s)	Calculated V_h (m/s)	$\frac{V_m}{V_h}$	μ
2000	106.9	3.0	6.2	0.48	0.028
2200	117.6	3.3	7.2	0.45	0.028
2400	128.3	3.9	8.3	0.46	0.030
2600	139.0	4.2	9.2	0.45	0.030
2800	149.7	4.6	9.1	0.50	0.031
3000	160.4	4.9	10.5	0.47	0.031
3200	171.1	5.4	11.6	0.47	0.032
3400	181.8	5.7	12.0	0.48	0.031

Table 5. Four-bladed rotor predicted conditions at 12.5 mbar.

RPM	V_{tip} (m/s)	Calculated V_h (m/s)	TBR $\frac{V_m}{V_h}$	Predicted V_m (m/s)	Predicted μ
2800	149.7	12.7	0.50	6.38	0.043
3000	160.4	13.8	0.47	6.49	0.040
3200	171.1	14.4	0.47	6.69	0.039
3400	181.8	15.2	0.48	7.21	0.040

EXPERIMENT VS. SIMULATIONS

This section presents plots of experimental results compared against RotCFD simulation for a two- and four-bladed rotor at terrestrial and Martian atmospheric densities.

RotCFD "turbulent" refers to the simulations in RotCFD using the aerodynamic coefficients generated from the "fully turbulent" flow type in C81Gen where the SA turbulence model is used. RotCFD "laminar" refers to the RotCFD simulations run with the aerodynamic coefficients obtained from the fully laminar flow type in C81Gen.

Two-bladed rotor at terrestrial atmospheric densities

Figures 29 to 31 show the experiment vs. simulation rotor performance plots for the two-bladed rotor at 1 atmosphere. At 1 atmosphere both two- and four-bladed rotor cases in RotCFD closely approximate the experimental trends. From the two-bladed rotor correlation with RotCFD, thrust is underpredicted by an average of around 8%, and torque and power are underpredicted by an average of roughly 5%.

Four-bladed rotor at terrestrial atmospheric densities

Figures 32 to 34 show the experiment vs. simulation rotor performance plots for the four-bladed rotor at 1 atmosphere. From the four-bladed rotor correlation with RotCFD, thrust differs from the experiment by around an average of 4%, and torque and power differ by an average of approximately 3%.

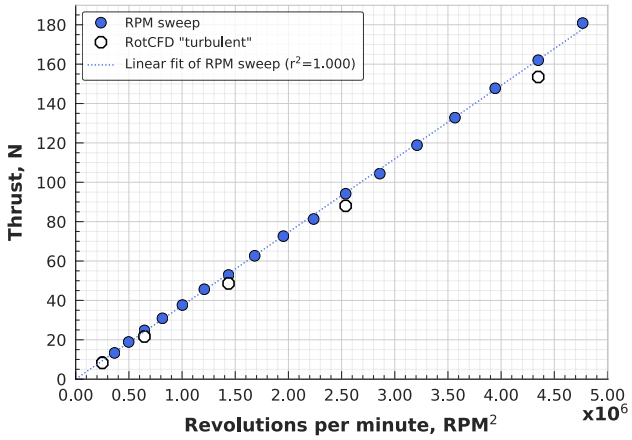

Figure 29. Experiment vs. simulations: plot of thrust vs. RPM² for the two-bladed rotor at 1 atmosphere.

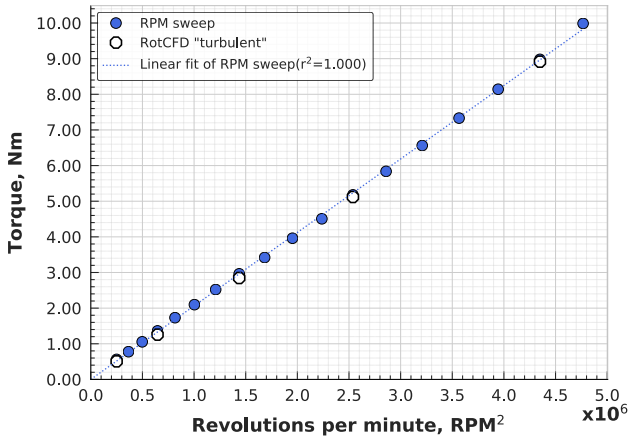

Figure 30. Experiment vs. simulations: plot of torque vs. RPM² for the two-bladed rotor at 1 atmosphere.

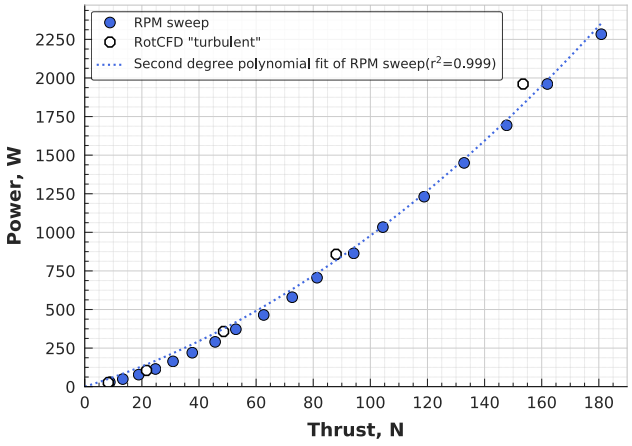

Figure 31. Experiment vs. simulations: plot of power vs. thrust for the two-bladed rotor at 1 atmosphere.

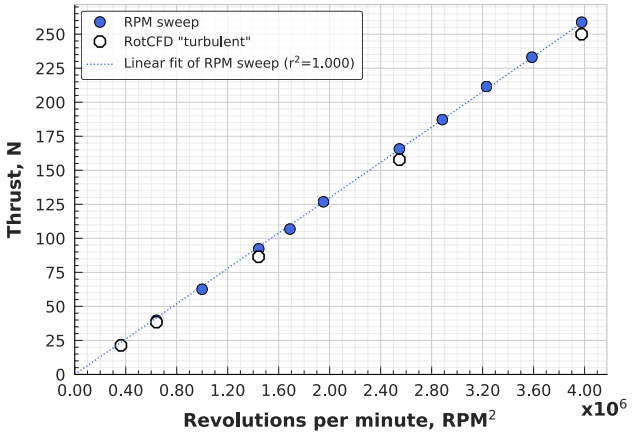

Figure 32. Experiment vs. simulations: plot of thrust vs. RPM² for the four-bladed rotor at 1 atmosphere.

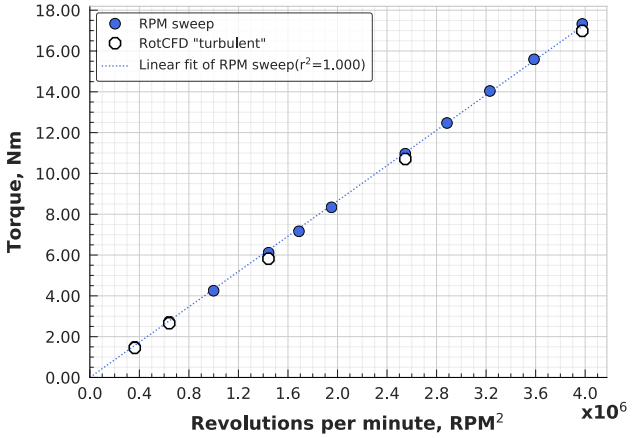

Figure 33. Experiment vs. simulations: Plot of torque vs. RPM² for the four-bladed rotor at 1 atmosphere.

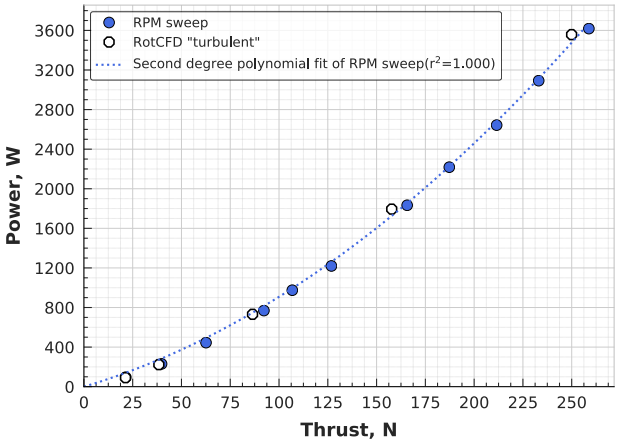

Figure 34. Experiment vs. simulations: Plot of power vs. thrust for the four-bladed rotor at 1 atmosphere.

Two-bladed rotor at Martian atmospheric densities

Figures 35 to 37 show the experiment vs. simulation rotor performance plots for the two-bladed rotor at Mars-like conditions.

RotCFD laminar simulations show a better correlation at reduced pressures for both rotor configurations when compared to the RotCFD “turbulent”. The RotCFD “turbulent” simulations overall underpredicted rotor performance. The greater discrepancy in prediction for both 10.7- and 12.5-mbar cases may be due to the airfoil aerodynamic coefficient tables (boundary layer transition behavior at such low Reynolds numbers), different facility effects at reduced pressure (wall boundary layer size, turbulence levels), or perhaps even inflow discrepancies in the predictions since the MARSWIT test section flow quality has never been characterized for this test configuration but was modeled as uniform.

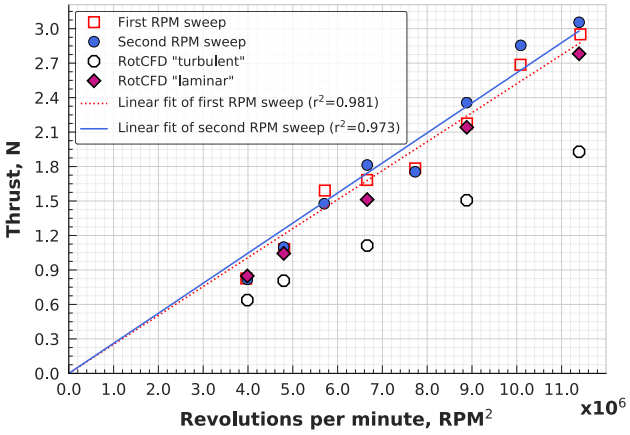

Figure 35. Experiment vs. simulations: plot of thrust vs. RPM² for the two-bladed rotor at 10.7 mbar.

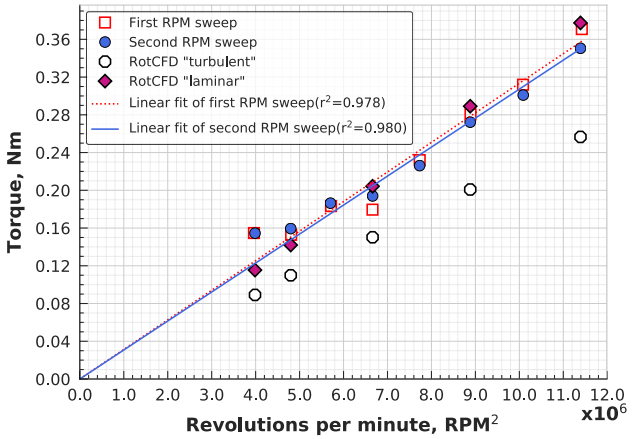

Figure 36. Experiment vs. simulations: plot of torque vs. RPM^2 for the two-bladed rotor at 10.7 mbar.

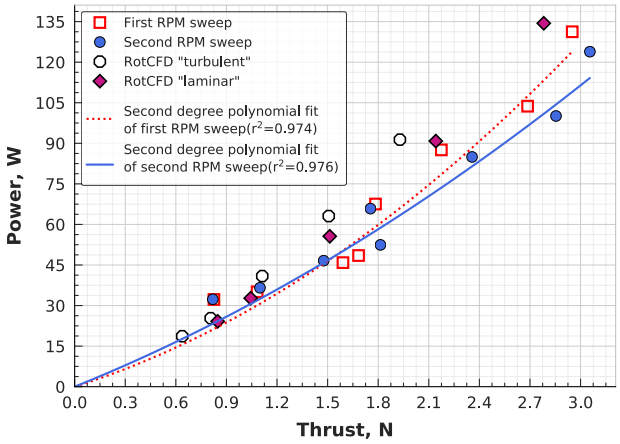

Figure 37. Experiment vs. simulations: plot of power vs. thrust for the two-bladed rotor at 10.7 mbar.

For the two-bladed rotor correlation with RotCFD "turbulent", thrust, torque and power is underpredicted by an average of around 30%. In the RotCFD "laminar" simulations the thrust differs by an average of approximately 7% for thrust and 10% for torque and power. However, it can be seen that the RotCFD "laminar" torque closely approximates the experimental linear trend.

Four-bladed rotor at Martian atmospheric densities

Figures 38 to 40 show the experiment vs. simulation rotor performance plots for the four-bladed rotor at Mars-like conditions.

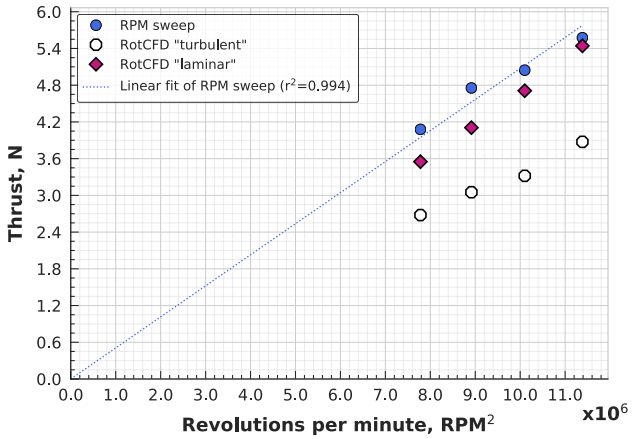

Figure 38. Experiment vs. simulations: plot of thrust vs. RPM^2 for the four-bladed rotor at 12.5 mbar.

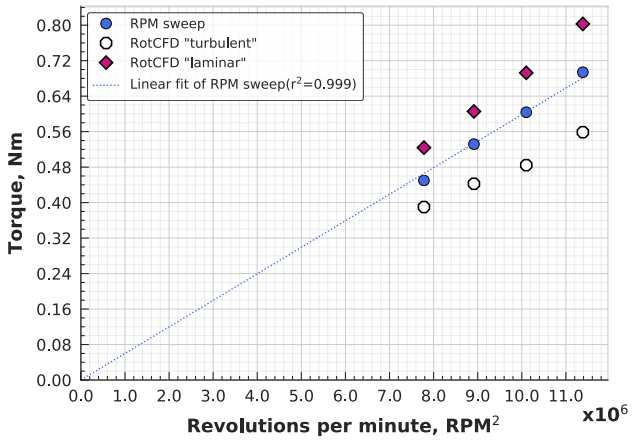

Figure 39. Experiment vs. simulations: plot of torque vs. RPM^2 for the four-bladed rotor at 12.5 mbar.

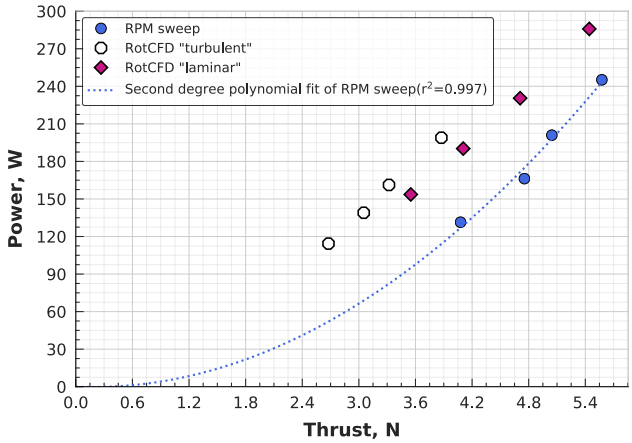

Figure 40. Experiment vs. simulations: plot of power vs. thrust for the four-bladed rotor at 12.5 mbar.

For the four-bladed rotor correlation with RotCFD "turbulent", thrust is underpredicted by an average of around 30%, and torque and power are underpredicted by an average of roughly 18%. RotCFD "laminar" underpredicts thrust by an average of roughly 9%, and torque and power are over predicted by approximately 15%.

Although the fully laminar flow type in C81Gen might be more representative of the flow type seen at such low Reynolds numbers, it might not be a proper fit for the interactions between the upper and lower rotors of the four-bladed rotor.

Airfoil Performance in C81Gen Simulations at Martian Atmospheric Densities

Figure 41 to 43 shows the C81Gen drag and lift coefficient results at Martian atmospheric densities for r/R=0.74 at Mach 0.2 and 0.5. This is exhibited to show the difference between the "fully turbulent" and fully laminar flow type at the lowest and highest Mach numbers that can be seen in this at this radial station. At these conditions, the operational chord based Reynolds number in this radial station ranges from around 3000 to 7000.

The two flow type solutions perform similarly at angles of attack of roughly -4 to 0 degrees. However, drag and lift coefficient are overall higher for the fully laminar flow solution with the exception of angles of attack lower than around -4 degrees where the lift coefficient is lower than the "fully turbulent" solution for both Mach numbers.

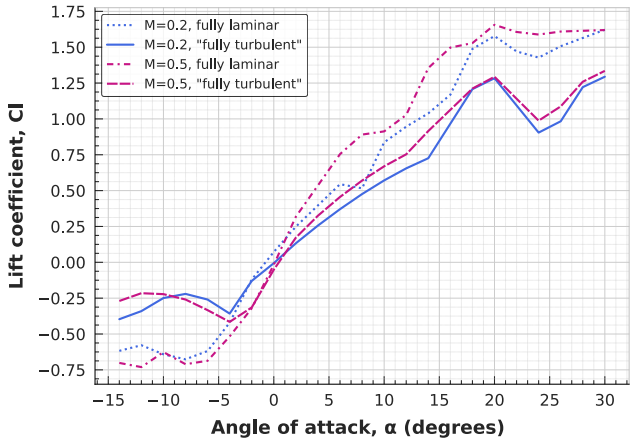

Figure 41 Lift coefficient vs. angle of attack at r/R=0.74

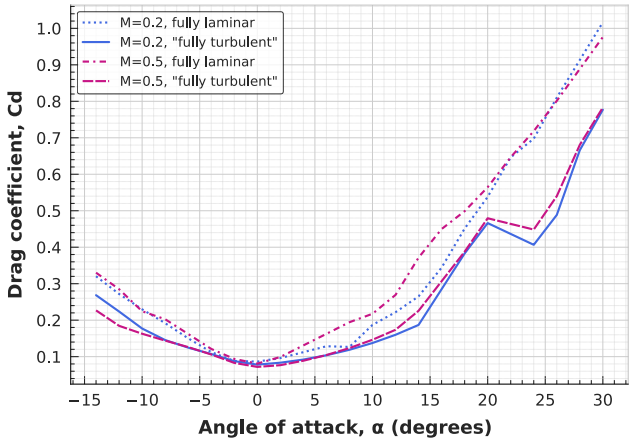

Figure 42 Drag coefficient vs. angle of attack at r/R=0.74

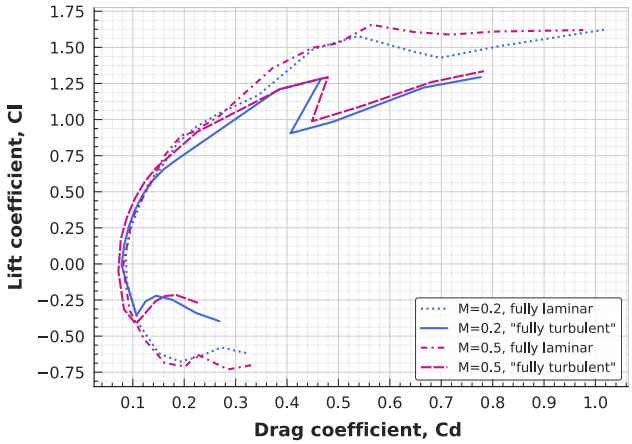

Figure 43 Lift coefficient vs. drag coefficient at r/R=0.74

Reynolds Number Effect on Rotor Performance

To study Reynolds number effect on rotor performance, data was collected during the pressure drift condition (at a drift rate of 1 mbar per minute). Figures 44 to 46 show the Reynolds number effect at 75% radial station ($Re_{0.75R}$) on figure of merit (*FM*), thrust coefficient (C_T), and power coefficient (C_P) when the two- and four-bladed rotors were spinning at 3000 RPM and at pressures ranging from 40 to 193 mbar.

Within this range of Reynolds numbers ($2\text{x}10^4$ to $9\text{x}10^4$), C_T and *FM* decrease around 26% and 36%, respectively when the Reynolds number decreases. Further, C_T and *FM* exhibited a second-degree polynomial trend for both rotor configurations when plotted against $Re_{0.75R}$. Moreover, C_P remained fairly constant, exhibiting variations of no more than 5.5%.

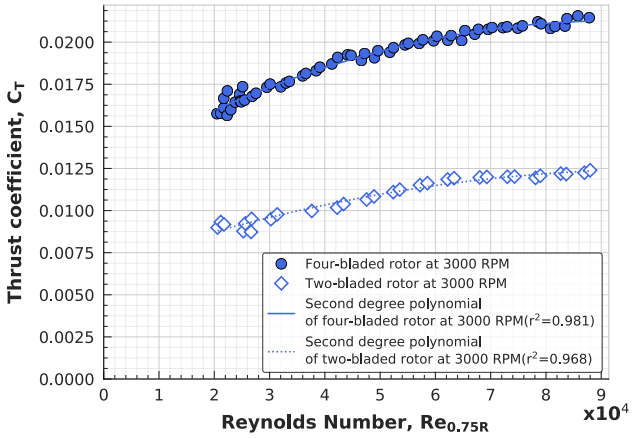

Figure 44. Reynolds number effect on thrust coefficient.

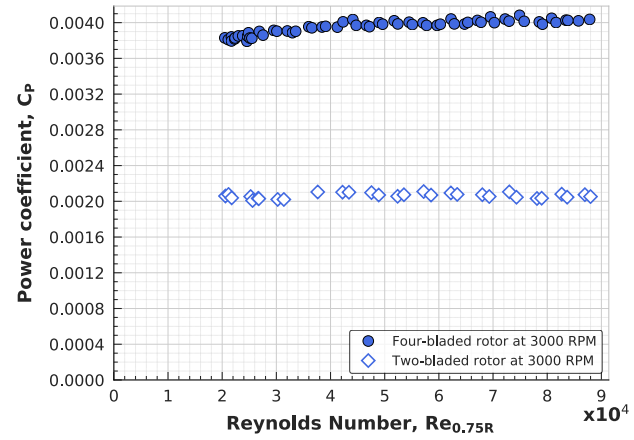

Figure 45. Reynolds number effect on power coefficient.

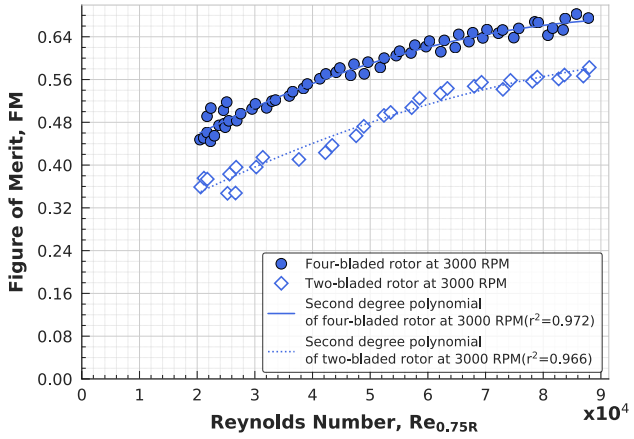

Figure 46 Reynolds number effect on figure of merit.

FUTURE WORK

Future work includes testing of the four-bladed rotor at Martian atmospheric densities while measuring wind tunnel speeds. Moreover, the same rotor configurations and test matrix executed for the forward flight testing will be performed outside the wind tunnel in a test stand to measure hover performance. Furthermore, hover experiments will be compared with CFD simulation results modeling hover operations.

CONCLUSIONS

Successful rotor testing operations measuring thrust, torque, power, and wind speed were demonstrated in the MARSWIT at Martian atmospheric densities and low speeds. Forward flight rotor performance was measured for a two- and four-bladed rotor at terrestrial and Martian (10.7 and 12.5 mbar) atmospheric density conditions. In addition, Reynolds number effect on rotor performance was presented for pressures ranging from 40 to 193 mbar. Repeatability at Mars-like conditions was demonstrated with the two-bladed rotor for thrust, torque, power, and wind speed measurements, where difference between the results exhibited an average of no more than 5%

Rotor performance for both rotor configurations is underpredicted overall in the RotCFD simulations at reduced pressures when using the airfoil aerodynamic coefficients obtained from the "fully turbulent" flow type simulation. Simulations exhibited a better correlation at Martian atmospheric densities when using airfoil aerodynamic coefficients obtained from the fully laminar flow type. The correlation with the two-bladed rotor shows that the fully laminar flow type in C81Gen might be more representative of the flow type seen at such low Reynolds numbers. However, it might not be a proper fit when considering the interactions between the upper and lower rotors of the four-bladed rotor. At 1 atmosphere, RotCFD results closely approximate to the experimental trends.

For Reynolds number from $2x10^4$ to $9x10^4$, the C_T and FM decreased around 26% and 36%, respectively when the Reynolds number decreased. Further, C_T and FM exhibited a second-degree polynomial trend for both rotor configurations when plotted against $Re_{0.75R}$. Moreover, C_P remained fairly constant, exhibiting variations of no more than 5.5%.

ACKNOWLEDGEMENTS

The author would like express her sincere thanks and gratitude to Dr. William Warmbrodt for his mentorship and tremendous support, Dr. Alan Wadcock for his continuous mentorship in testing and analysis, Farid Haddad for his expertise in electronics and controls during experimental setup, Ken Smith for operation of the PAL vacuum facility,

Larry Meyn for the data reduction, Larry Young for originally inspiring the idea of forward flight testing under Martian conditions, Witold Koning for his mentorship in aerodynamics and CFD simulations, Kristen Kallstrom and Haley Cummings for their invaluable feedback. Also, the author would like to thank the 2018 Aeromechanics interns that provided their assistance for experimental testing. Finally, a special thanks to Geoffrey Ament for his outstanding mentorship.

REFERENCES

[1] J. (Bob) Balaram *et al.*, "Mars Helicopter Technology Demonstrator," *AIAA Science and Technology Forum and Exposition (AIAA SciTech), Kissimmee, FL*, 2018.

[2] H. F. Grip *et al.*, "Guidance and Control for a Mars Helicopter," *AIAA Science and Technology Forum and Exposition (AIAA SciTech), Kissimmee, FL*, 2018.

[3] L. A. Young, E. W. Aiken, M. Derby, R. Demblewski, and J. Navarrete, "Experimental Investigation and Demonstration of Rotary-Wing Technologies for Flight in the Atmosphere of Mars," *Proceedings of the 58th Annual Forum of the American Helicopter Society*, 2002.

[4] M. Anyoji, D. Numata, H. Nagai, and K. Asai, "Effects of Mach Number and Specific Heat Ratio on Low-Reynolds-Number Airfoil Flows," *AIAA Journal*, vol. 53, no. 6, pp. 1640–1654, 2015.

[5] W. J. F. Koning and W. Johnson, "Improved Mars Helicopter Aerodynamic Rotor Model for Comprehensive Analyses," pp. 1–14, 2018.

[6] G. A. Ament and W. J. F. Koning, "Isolated Rotor Forward Flight Testing From One Atmosphere Down to Martian Atmospheric Densities," *AHS International Technical Conference on Aeromechanics Design for Transformative Vertical Flight, San Francisco, CA*, 2018.

[7] "NASA - Planetary Aeolian Laboratory." [Online]. Available: https://www.nasa.gov/centers/ames/business/planetary_aeolian_facilities.html. [Accessed: 21-Dec-2018].

[8] "PAL | The Ronald Greeley Center for Planetary Studies." [Online]. Available: https://rpif.asu.edu/index.php/pal/. [Accessed: 21-Dec-2018].

[9] M. McCoy, A. J. Wadcock, and L. A. Young, "Documentation of the Recirculation in a Closed-Chamber Rotor Hover Test," NASA/TM-2016-219162, Aug. 2016.

[10] W. J. F. Koning, "Generation of Performace Model for the Aeolian Wind Tunnel (AWT) Rotor at Reduced Pressure," NASA/CR-2018-219737, Jan. 2018.

[11] L. A. Young *et al.*, "Engineering Studies into Vertical Lift Planetary Aerial Vehicles," *AHS International Meeting on Advanced Rotorcraft Technology and Life Saving Activities, Utsunomiya, Tochigi, Japan*, 2002.

[12] R. G. Rajagopalan *et al.*, "RotCFD - A Tool for Aerodynamic Interference of Rotors: Validation and Capabilities," *American Helicopter Society International – Future Vertical Lift Aircraft Design Conference, San Francisco, CA*, 2012.

[13] L. A. Young, G. K. Yamauchi, and G. Rajagopalan, "Simulated Rotor Wake Interactions Resulting From Civil Tiltrotor Aircraft Operations Near Vertiport Terminals," *American Institute of Aeronautics and Astronautics*, 2013.

[14] W. J. F. Koning, C. W. Acree, and G. Rajagopalan, "Using RotCFD to Predict Isolated XV-15 Rotor Performance," *American Helicopter Society International – AHS Specialists' Conference on Aeromechanics Design for Vertical Lift*, 2016.

[15] W. J. F. Koning, W. Johnson, and B. G. Allan, "Generation of Mars Helicopter Rotor Model for Comprehensive Analyses," *AHS Specialists' Conference on Aeromechanics Design for Transformative Vertical Flight, San Francisco, CA*, 2018.

[16] S. F. Hoerner, "Fluid-Dynamic Drag: Practical Information on Aerodynamic Drag and Hydrodynamic Resistance". Hoerner Fluid Dynamics, 1965.

[17] B. N. Perez Perez, "Rotor CFD Analysis at Terrestrial and Martian Atmospheric Densities," NASA/CR–2018–219780, Sept. 2018.

[18] B.N. Perez Perez, G. A. Ament and W. J. F. Koning "Experimental Forward Flight Rotor Performance Testing From Terrestrial to Martian Atmospheric Densities," NASA/CR–2019–20229.

[19] G. A. Ament and W. J. F. Koning and B.N. Perez Perez "Isolated Rotor Forward Flight Testing at Martian Atmospheric Density Data Report," NASA/CR–2018–219736.

[20] F. J. Argus, G. A. Ament, and W. J. F. Koning, "The Influence of Laminar-Turbulent Transition on Rotor Performance at Low Reynolds Numbers," in *VFS Technical Meeting on Aeromechanics for Advanced Vertical Flight*, San Jose, CA, 2020.